NEUTRONICS BENCHMARK OF CEFR START-UP TESTS: *reaction rates and integral reactivity coefficients*

T. K. Kim, M. Jarrett
Argonne National Laboratory
Argonne, IL. U.S.A
tkkim@anl.gov

P. Sciora
French Alternative Energies and Atomic Energy Commission (CEA)
France

K. Devan, S. V. Vedharathinam
Indira Gandhi Centre for Atomic Research (IGCAR)
India

C. Batra, V. Kriventsev
International Atomic Energy Agency
Vienna, Austria

J. Bodi, K. Mikityuk
Paul Scherrer Institute
Switzerland

Youqi Zheng, Xianan Du
School of Nuclear Science and Technology, Xi'an Jiaotong University
Xi'an, China

Deokjung Lee, Tuan Quoc Tran, Jiwon Choe
Ulsan National Institute of Science and Technology
Republic of Korea

H. Taninaka
Japan Atomic Energy Agency
Japan

A. Gómez-Torres, R. López-Solís, J. Galicia-Aragon, E. del Valle-Gallegos
National Institute of Nuclear Research
Mexico

S. Di Pasquale, V. Giusti, A. Petruzzi
Nuclear and Industrial Engineering and University of Pisa
Italy

Abstract

A coordinated research project (CRP) entitled "Neutronics Benchmark of CEFR Start-up Tests" has been conducted for improvement of analytical capabilities of fast reactor modelling and simulations. Among the six experiments and two numerical benchmarks, two benchmarks of reaction rate measurements from foil activations and the integral reactivity coefficient are documented in this paper. Sixteen and ten international organizations participated in the reaction rate benchmark and evaluation of integral reactivity coefficients, respectively, using various deterministic and stochastic computation codes and evaluated nuclear data libraries of ENDF/B, JEFF, and JENDL. For the reaction rate measurement by foil activations, stochastic and deterministic codes used in this study gives results in good agreement with the experiment, axially and radially. However, a relatively large variation is observed in the estimated ^{197}Au (n, γ) reaction rate values , in particular, at points far from the fueled-region. Except for several outliers, the evaluated integral reactivity coefficients show generally good agreement between participants regardless of deterministic and stochastic calculation methods.

1. INTRODUCTION

China Experimental Fast Reactor (CEFR) is a 65 MW pool-type sodium-cooled fast reactor with highly enriched uranium dioxide fuels and stainless-steel reflectors. CEFR reached the first criticality in 2010 and conducted multiple experiments as start-up physics tests, including measurements of criticality, control rod worth, reactivity coefficients, foil activations, etc. The experiments made an essential part of the reactor start-up procedures, but the results can also be utilized to validate modelling and simulation capabilities for SFR design and analysis. Under the framework of coordinated research activities of the International Atomic Energy Agency (IAEA), the China Institute of Atomic Energy (CIAE) proposed a coordinated research project (CRP) entitled "Neutronics Benchmark of CEFR Start-up Tests," targeting for improvement of member countries' analytical capabilities in the field of fast reactor modelling and simulations.

About 30 international organizations from multiple member countries are participating at the CRP. CIAE has proposed detailed design parameters of the CEFR (i.e., dimensions, compositions, uncertainties, etc.) and experiment information and measurements, and the benchmark specifications have been finalized by joint efforts of participants [1]. The benchmark consists of six experiments, including criticality per fuel loading, control rod worth measurement, sodium void reactivity, temperature reactivity, subassembly swap reactivity, and foil activation measurement. Participants also agreed on two more numerical benchmarks of the evaluation of integral reactivity coefficients and analyses of sensitivity and uncertainty propagation for understanding the integral safety feature of the CEFR even though those have not been measured in the CEFR start-up tests.

Among eight benchmark items, reaction rate measurements from foil activations and the integral reactivity coefficient are documented in this paper. The CRP consists of two benchmark steps: blind benchmark without measured data from the CEFR start-up test and open benchmark with measured data. In the open benchmark, all participants could access the measured data and refined the calculations when there were discrepancies between the calculated results and measured data. The results of the open benchmark were compared in this paper.

2. REACTION RATES

2.1. Measurement of reaction rates in CEFR

The neutron activation measurements were performed with the help of specially manufactured experimental subassemblies having provisions to insert and withdraw an irradiation device loaded with activation foils/balls. The special subassembly meant for loading in the fissile zone was similar to a fuel assembly in which 7 fuel pins at the centre were removed. Similarly, a reflector assembly with empty central pin was also used for reaction rate measurements in the reflector zone. For this benchmark, six different reactions were studied: ^{235}U (n, f), ^{238}U (n, f), ^{237}Np (n, f), ^{197}Au (n, γ), ^{58}Ni (n, p), ^{27}Al (n, α). These foils were selected based on their responses to neutron spectrum.

The activation foils were introduced into the core by loading an experimental fuel or steel subassembly depending on the measurement position; fissile or reflector zone. After placing the special subassembly and foils, irradiation power was attained, and reactor kept in critical state for 2 hours. After irradiation, the reactor was shut down quickly by rod-drop. As only one special subassembly each (fuel and stainless steel) were available, a power monitoring foil was kept in a neutral position in order to account for minor variations in power and the required normalization thereafter. This step is irrelevant in the simulation part. Radial reaction rate distribution was measured by placing the foils at eight different radial positions; five in the fissile zone and three in the reflectors (Fig. 1). Axial reaction rate distribution was measured at only one position (2-2); 13 to 14 axial positions from lower interface of fertile blanket to the top of the sodium plenum zone, including fissile zone, upper fertile blanket, upper gas plenum and plug. Activities of the irradiated foils/balls were measured with a high purity germanium detector to deduce the reaction rate.

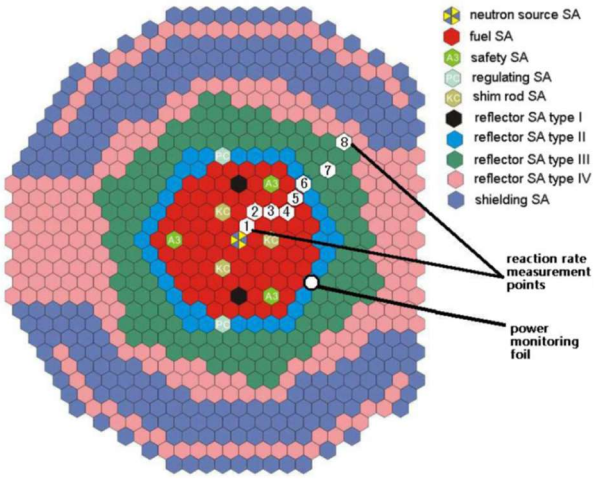

FIG. 1. Radial positions for irradiation foils

2.2. Comparison of reaction rates

The reaction rates, normalized to that of a reference point (i.e., at position no. 1 (2-2) for radial and at -40 mm or -32 mm axial position with respect to core centre, depending on the type of reaction rates, for axial), were computed by all the participants for comparison. This work package was analysed by 16 organisations and the details of institution, codes and library used are presented in Table 1. This benchmark was separated into two phases. The first one, the blind phase, was analysed by some participants without the knowledge of experimental values and the exact geometry description of the foils. The second phase, the refined phase, was done after knowing the exact geometrical description of foils and the experimental values. Not all participants produced results for refined phase. In such cases, blind phase results are interpreted here as refined phase results also.

TABLE 1. LIST OF PARTICIPANTS TO REACTION RATE EVALUATIONS

Country	Organization	Code	Library	Blind phase	Deter-ministic	Stochastic
China	INEST	SuperMC	HENDL-3.0	X		X
China	CIAE	NAS, RMC	ENDF/B-VIII.0	X	X	X
China	XJTU	SARAX	ENDF/B-VIII.0		X	
France	CEA	ERANOS [2]	JEFF 3.1 [3]	X	X	X
Germany	HZDR	Sepent	JEFF 3.1			X
Hungary	MTA / CER	Sepent	ENDF/B-VIII.0	X		X
India	IGCAR	OpenMC [4]	ENDF/B-VIII.0	X		X
Italy	NINE/UNIPI	Sepent	ENDF/B-VIII.0			X
Japan	JAEA	PARTISN, MVP	JENDL-4.0		X	X
Korea	UNIST	MCS	ENDF/B-VII.1	X		X
Korea	KAERI	DIF3D, McCARD	ENDF/B-VII.0 ENDF/B-VII.1	X	X	 X
Mexico	ININ	Sepent, Aznhex	ENDF/B-VIII.0			X
Romania	RATEN (ICN)	MCNP	ENDF/B-VIII.0	X		X
Russia	NRCKI	JARFR, Sepent	ABBN-93,JEFF 3.3		X	X
Slovakia	VUJE	Sepent	ENDF/B-VII.0	X		X
U.S.A	ANL	DIF3D	ENDF/B-VII.0	X	X	

The relative deviation of the participant results from the experimental values are presented in Fig 2 for each reaction rate. CIAE estimated the experimental uncertainties between 15% and 20%. Most of the simulation results are within the range of this uncertainty in the fissile zone. The most chaotic distribution of results in this zone can be seen in the case of ^{27}Al reaction rate, because of the low absolute value obtained, in comparison with the other reaction rates.

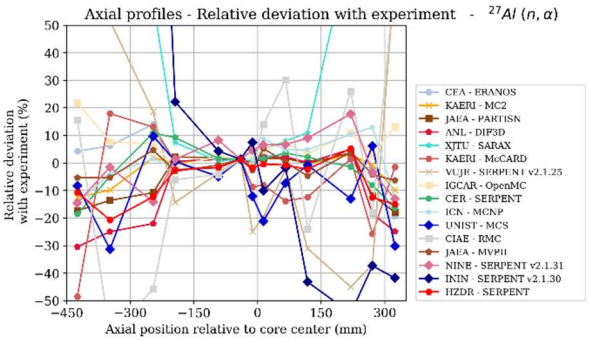
Axial profiles - Relative deviation with experiment - ^{27}Al (n,α)
Relative deviation with experiment (%)
Axial position relative to core center (mm)
CEA - ERANOS
KAERI - MC2
JAEA - PARTISN
ANL - DIF3D
XJTU - SARAX
KAERI - McCARD
VUJE - SERPENT v2.1.25
IGCAR - OpenMC
CER - SERPENT
ICN - MCNP
UNIST - MCS
CIAE - RMC
JAEA - MVPII
NINE - SERPENT v2.1.31
ININ - SERPENT v2.1.30
HZDR - SERPENT

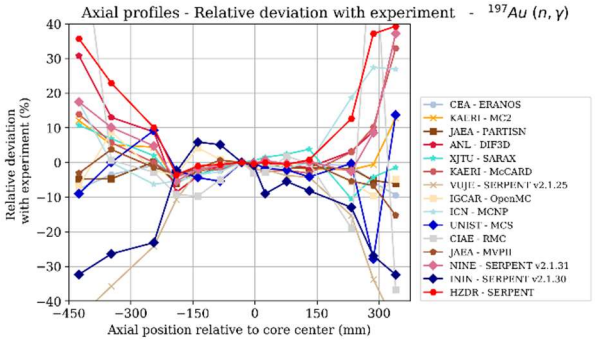
Axial profiles - Relative deviation with experiment - ^{197}Au (n,γ)
Relative deviation with experiment (%)
Axial position relative to core center (mm)
CEA - ERANOS
KAERI - MC2
JAEA - PARTISN
ANL - DIF3D
XJTU - SARAX
KAERI - McCARD
VUJE - SERPENT v2.1.25
IGCAR - OpenMC
ICN - MCNP
UNIST - MCS
CIAE - RMC
JAEA - MVPII
NINE - SERPENT v2.1.31
ININ - SERPENT v2.1.30
HZDR - SERPENT

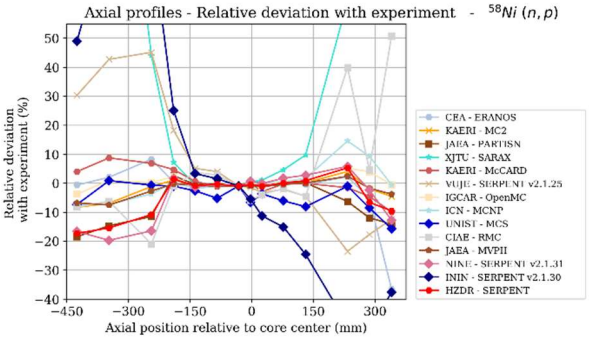
Axial profiles - Relative deviation with experiment - ^{58}Ni (n,p)
Relative deviation with experiment (%)
Axial position relative to core center (mm)
CEA - ERANOS
KAERI - MC2
JAEA - PARTISN
XJTU - SARAX
KAERI - McCARD
VUJE - SERPENT v2.1.25
IGCAR - OpenMC
ICN - MCNP
UNIST - MCS
CIAE - RMC
JAEA - MVPII
NINE - SERPENT v2.1.31
ININ - SERPENT v2.1.30
HZDR - SERPENT

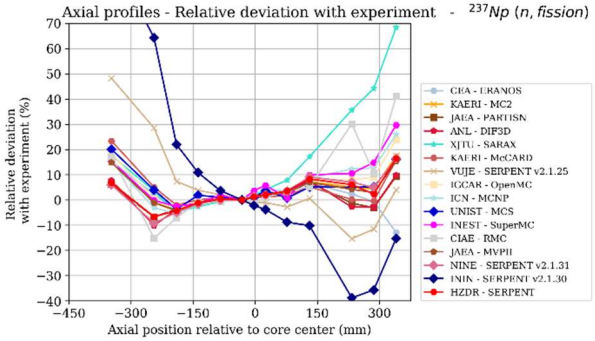
Axial profiles - Relative deviation with experiment - ^{237}Np $(n,fission)$
Relative deviation with experiment (%)
Axial position relative to core center (mm)
CEA - ERANOS
KAERI - MC2
JAEA - PARTISN
ANL - DIF3D
XJTU - SARAX
KAERI - McCARD
VUJE - SERPENT v2.1.25
IGCAR - OpenMC
ICN - MCNP
UNIST - MCS
INEST - SuperMC
CIAE - RMC
JAEA - MVPII
NINE - SERPENT v2.1.31
ININ - SERPENT v2.1.30
HZDR - SERPENT

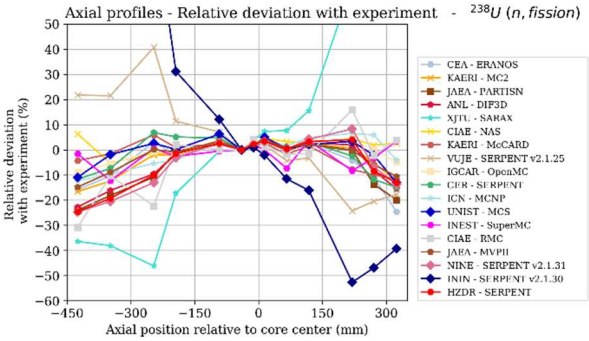
Axial profiles - Relative deviation with experiment - ^{238}U $(n,fission)$
Relative deviation with experiment (%)
Axial position relative to core center (mm)
CEA - ERANOS
KAERI - MC2
JAEA - PARTISN
ANL - DIF3D
XJTU - SARAX
CIAE - NAS
KAERI - McCARD
VUJE - SERPENT v2.1.25
IGCAR - OpenMC
CER - SERPENT
ICN - MCNP
UNIST - MCS
INEST - SuperMC
CIAE - RMC
JAEA - MVPII
NINE - SERPENT v2.1.31
ININ - SERPENT v2.1.30
HZDR - SERPENT

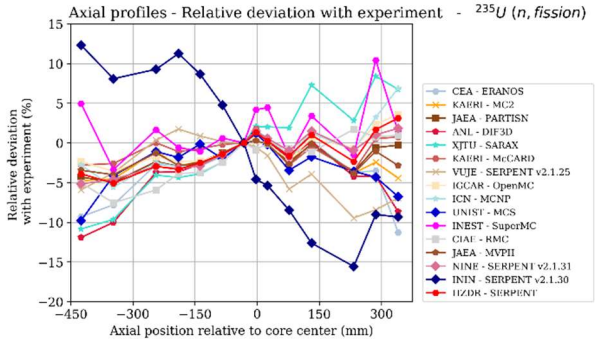
Axial profiles - Relative deviation with experiment - ^{235}U $(n,fission)$
Relative deviation with experiment (%)
Axial position relative to core center (mm)
CEA - ERANOS
KAERI - MC2
JAEA - PARTISN
ANL - DIF3D
XJTU - SARAX
KAERI - McCARD
VUJE - SERPENT v2.1.25
IGCAR - OpenMC
ICN - MCNP
UNIST - MCS
INEST - SuperMC
CIAE - RMC
JAEA - MVPII
NINE - SERPENT v2.1.31
ININ - SERPENT v2.1.30
HZDR - SERPENT

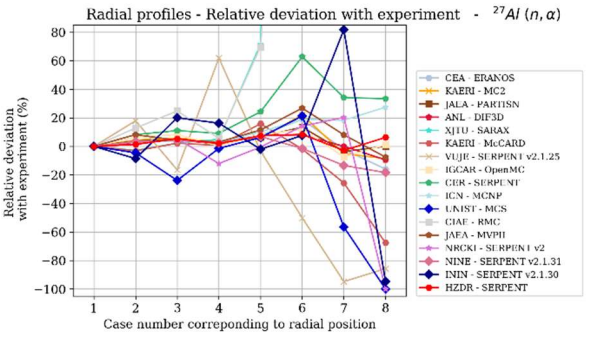
Radial profiles - Relative deviation with experiment - ^{27}Al (n,α)
Relative deviation with experiment (%)
Case number correponding to radial position
CEA - ERANOS
KAERI - MC2
JALA - PARTISN
ANL - DIF3D
XJTU - SARAX
KAERI - McCARD
VUJE - SERPENT v2.1.25
IGCAR - OpenMC
CER - SERPENT
ICN - MCNP
UNIST - MCS
CIAE - RMC
JAEA - MVPII
NRCKI - SERPENT v2
NINE - SERPENT v2.1.31
ININ - SERPENT v2.1.30
HZDR - SERPENT

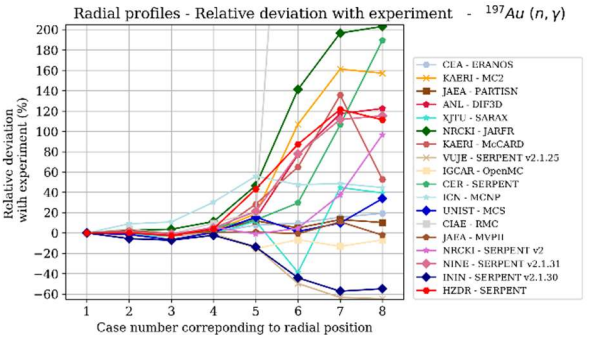
Radial profiles - Relative deviation with experiment - ^{197}Au (n,γ)
Relative deviation with experiment (%)
Case number correponding to radial position
CEA - ERANOS
KAERI - MC2
JAEA - PARTISN
ANL - DIF3D
XJTU - SARAX
NRCKI - JAERI
KAERI - McCARD
VUJE - SERPENT v2.1.25
IGCAR - OpenMC
CER - SERPENT
ICN - MCNP
UNIST - MCS
CIAE - RMC
JAEA - MVPII
NRCKI - SERPENT v2
NINE - SERPENT v2.1.31
ININ - SERPENT v2.1.30
HZDR - SERPENT

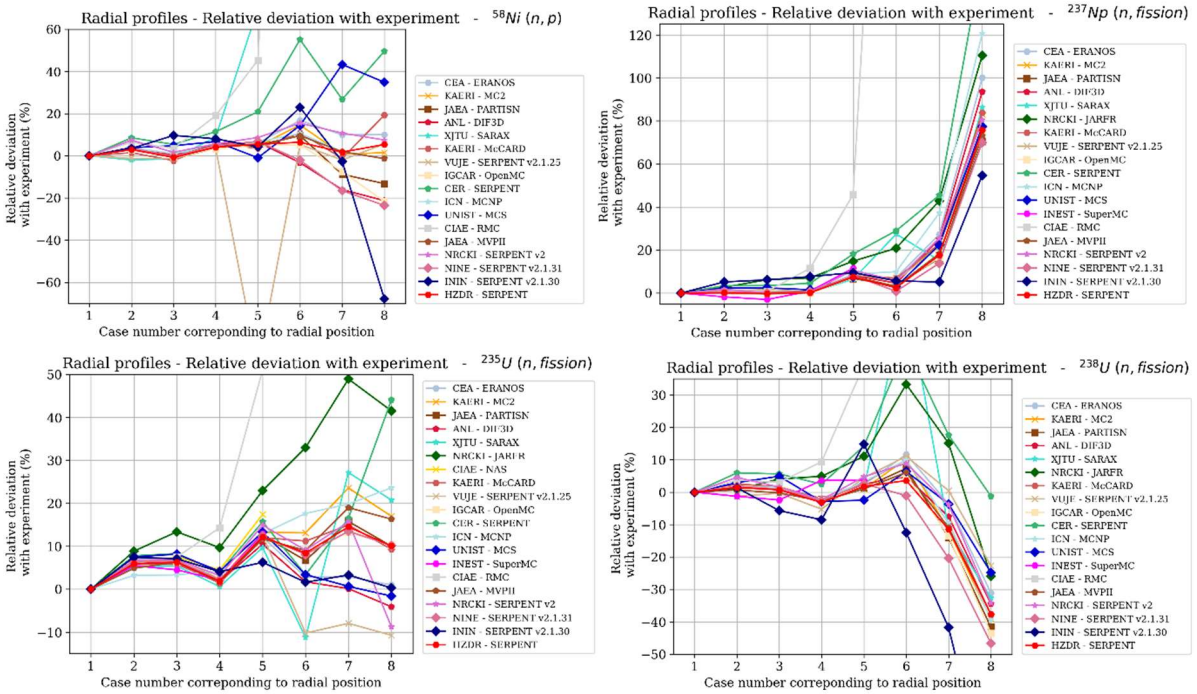

FIG. 2. Comparison of reaction rates (Top: axial distribution, bottom: radial distribution)

In the non-fissile zones, disagreements are seen for most of the codes.

- For stochastic codes, good agreement is seen among some codes because of good convergence, whereas some had chaotic distribution due to high statistical error. In the refined phase, some participants improved their statistics, and their results are seen converging within the common band of results. However, in the non-fissile zone, it is difficult to see a better agreement between codes within 20%.
- With deterministic codes, deviation is similar, but it is very difficult to see a good agreement between all the codes in non-fissile zones. Better cross-sections with sufficient number of energy groups might be needed to account for neutron transport and leakage effects.

Radially, some calculated points are not coherent with the experiment: positions #7 and #8 with ^{237}Np, and position #8 with ^{238}U. However, the codes present a good agreement between them. There might be a problem with the experimental value, or a significant simplification in the model defined for this benchmark.

With respect to ^{197}Au simulations, only few participants have produced results with good agreement to measured values. This might be attributed to the exact foil dimensions not being used in stochastic codes or self-shielding not being accounted properly in deterministic codes.

3. INTEGRAL REACTIVITY COEFFICIENTS

3.1. Definition of integral reactivity coefficients

The integral reactivity coefficients have been defined by perturbating various parameters from the normal operation condition at cold state (250 ºC). The normal operation core layout, material compositions, and control rods at critical state are provided in the CEFR benchmark technical specification.

Axial and radial expansion reactivity coefficients are defined by the core multiplication change from the normal state to the 1% expanded states,

$$\Delta\rho^{exp.}(\frac{pcm}{\%}) = \frac{k^{exp.} - k^{normal}}{1\%\ expansion},$$

where $k^{exp.}$ and k^{normal} denote the core multiplication factors at the expanded and normal states, respectively. Because fresh pellets are freely movable in cladding, it was assumed that only both fuel and blanket pellets are axially expanded by 1% and other structures (cladding, duct, etc.) are not axially expanded. For the radial

expansion, it was assumed that the radial expansion is dictated by the grid plate and all subassemblies in the core are uniformly expanded radially by 1%.

Density reactivity coefficients of sodium, steel, and fuel are defined by the core multiplication change from the normal state to the density perturbed states;

$$\Delta\rho^{density}\left(\frac{pcm}{\%}\right) = \frac{k^{density} - k^{normal}}{1\%\ or\ 10\%\ density\ chang},$$

where $k^{density}$ is the core multiplication factor of the density perturbed state. The density perturbed state is defined by 1% density increase in sodium and fuel (including upper blanket) pellet, but the steel density is increased by 10%. For simplicity, it was assumed that the density changes are only happened in 79 fuel subassemblies (i.e., densities of other subassemblies are not changed).

Doppler constants at normal and flowing sodium voided states are defined by the core multiplication change from the normal state to fuel temperature perturbed states;

$$\Delta\rho^{doppler}_{normal}\left(\frac{pcm}{\Delta T}\right) = \frac{k^{high\ temp.}_{normal} - k^{normal}}{250\ K\ temperature\ chang},$$

$$\Delta\rho^{doppler}_{voided}\left(\frac{pcm}{\Delta T}\right) = \frac{k^{high\ temp.}_{voided} - k^{normal}_{voided}}{250\ K\ temperature\ change},$$

where $k^{high\ temp.}_{normal}$, $k^{high\ temp.}_{voided}$, and $k^{normal.}_{voided}$ denote the core multiplication factors with high fuel temperature at the normal condition, high fuel temperature at the voided condition, and normal operating temperature at voided condition, respectively. For the fuel temperature perturbed case, the fuel temperature is increased to 500 °C. The sodium voided state is defined by the voided condition of flowing sodium inside duct of 79 fuel subassemblies from Lower Connector to Handling Head. Thus, the sodium in inter-fuel assemblies (i.e., outside of duct of fuel assemblies) and the sodium in non-fuel assemblies are not voided.

Finally, control rod expansion reactivity coefficients are defined by the core multiplication change from the normal state to the 10 cm control rod (CR) insertion by CR expansion,

$$\Delta\rho^{CR}_{regulating}\left(\frac{pcm}{cm}\right) = \frac{k^{CR\ insertion}_{regulating\ or\ shim} - k^{normal}}{10\ cm\ CR\ insertion},$$

where $k^{CR\ insertion}_{regulating,shim}$ is the core multiplication factor when regulating or shim CRs are inserted by 10 cm from the original critical positions. In the evaluation integral reactivity coefficient, the appropriate adjustment of solid material densities is required to conserve the original loads in the perturbed states.

3.2. Comparison of integral reactivity coefficients

The integral reactivity coefficients calculated by deterministic and stochastic codes are compared in this section. Figure 3 shows the axial and radial expansion coefficients. The values obtained from deterministic and stochastic methods are plotted with blue and orange colors for comparison purpose. IGCAR(E) and IGCAR(J) indicate the results using the nuclear data library of ENDF/B-VIII.0 and JEFF 3.3, respectively. CEFR has expansion coefficients, and the most probable axial and radial expansion coefficients are about -355 pcm/%-expansion and -885 pcm/%-expansion, respectively.

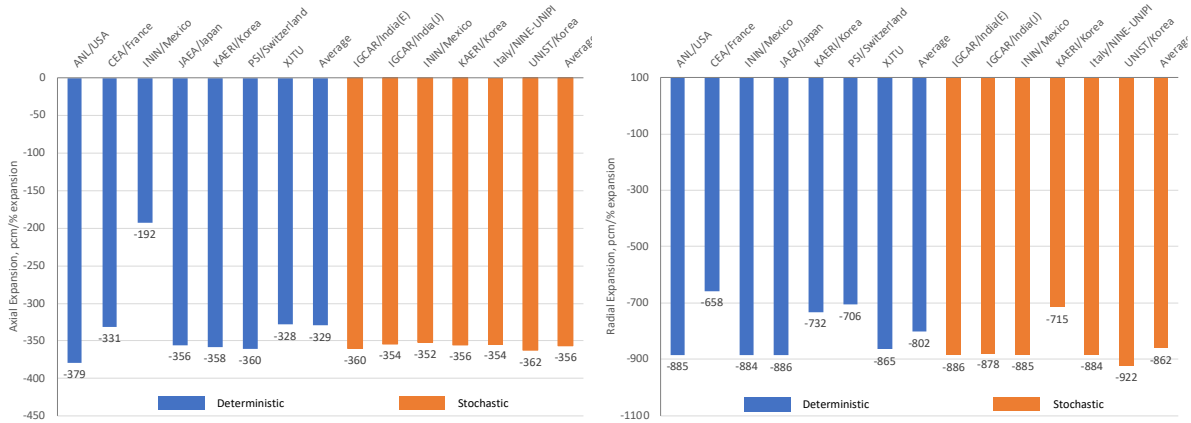

FIG. 3 Axial (left) and radial (right) expansion coefficients (pcm/%-expansion)

The density coefficients of fuel, steel, and sodium are compared in Fig. 4. CEFR has positive density coefficients for three materials. In particular, highly enriched uranium oxide fuel and leaky core configuration

increase the reactivity per increase in sodium density. Except for one result in stochastic calculations, there is good agreement of the fuel density coefficients. The average fuel density coefficients are 550 pcm/%-density-increase and 548 pcm/%-density-increase for the deterministic and stochastic calculations, respectively. For steel density coefficient, deterministic results are slightly more positive than the stochastic results. Except for few outlier results, the sodium density coefficients of both deterministic and stochastic results are within 31- 35 pcm/%-density-increase.

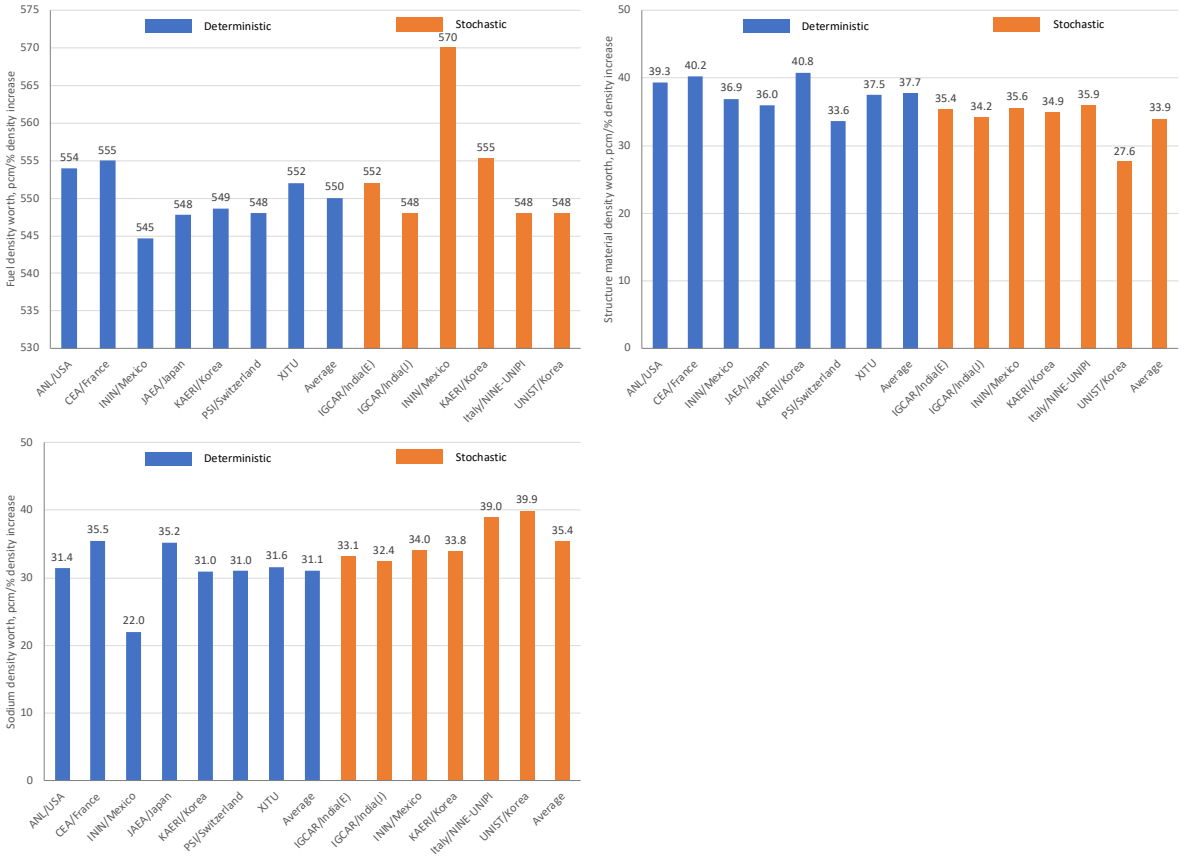

FIG. 4 Fuel (upper left), steel (upper right), and sodium (bottom) density coefficients (pcm/%density increase)

Doppler constants at normal and sodium voided conditions are compared in Fig. 5. For Doppler constant at normal condition, both deterministic and stochastic results are agreed well at about -0.18 pcm/K, while Doppler constant at sodium voided condition has relatively large deviations. Compared to Doppler constants at normal condition, Doppler constant at sodium voided condition is slightly less negative because of the reduced Doppler effect with hardened neutron spectrum.

The regulating and shim control rod expansion coefficients are compared in Fig. 6. The average regulating control rod expansion coefficients are -8.4 pcm/cm-insertion and -7.7 pcm/cm-insertion for deterministic and stochastic calculations, respectively. The average shim control rod has much more negative expansion coefficients.

Generally, the deterministic results have relatively large standard deviations compared to the stochastic results. For instance, the standard deviations of stochastic results are generally less than 10% (except for Doppler constants), while the standard deviations of deterministic results are larger than 10% (except for fuel density coefficient and regulating control rod worth). Wide diversity of deterministic methods could be a reason of the larger deviation in the deterministic results.

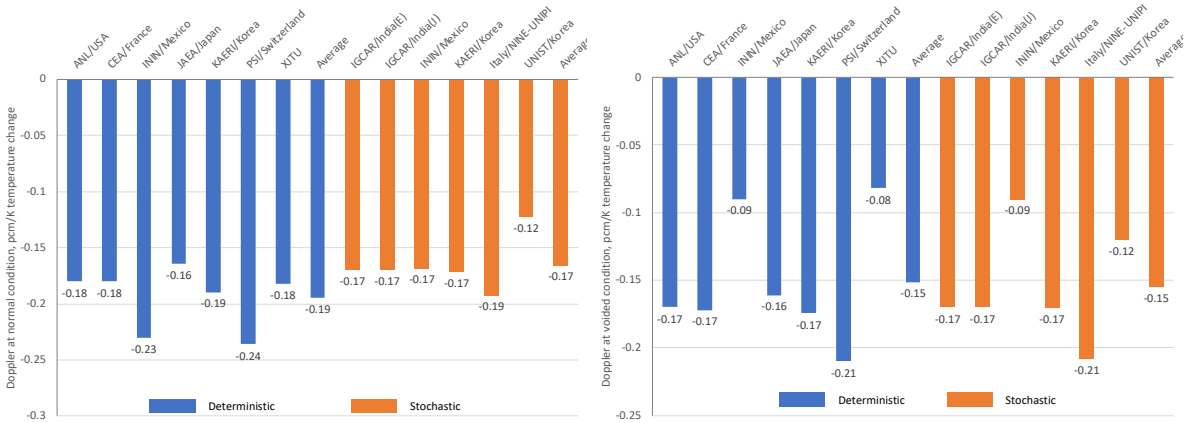

FIG. 5 Doppler constant at normal (left) and sodium voided (right) conditions

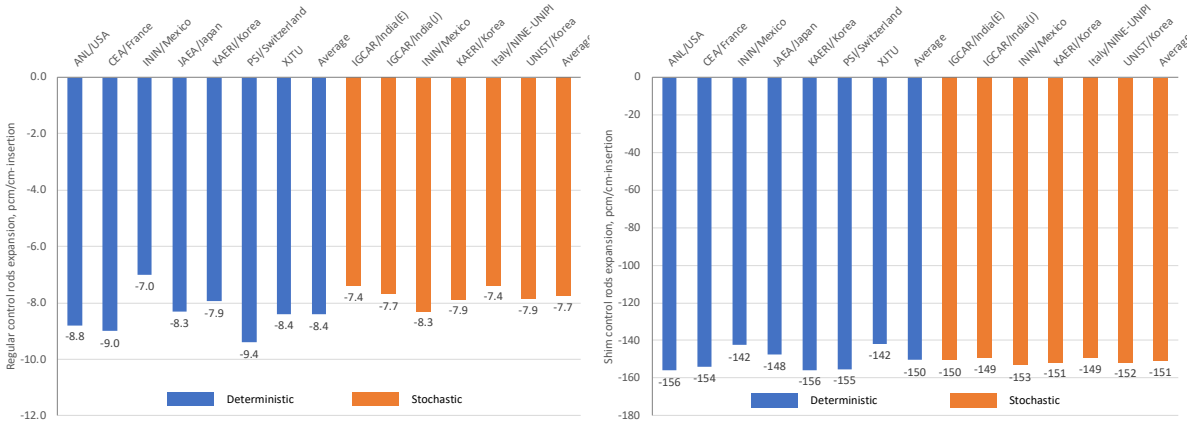

FIG. 6 Regulating (left) and shim (right) control rods expansion coefficients

4. CONCLUSIONS

A coordinated research project (CRP) entitled “Neutronics Benchmark of CEFR Start-up Tests” has been initiated under the framework of coordinated research activities of the International Atomic Energy Agency (IAEA). The primary objective of the CRP is to improve analytical capabilities of member countries in the field of fast reactor modelling and simulations by comparing calculated results with measured values in the CEFR start-up tests. The benchmark consists of six experiments and two numerical calculations, including criticality per fuel loading, control rod worth measurement, sodium void reactivity, temperature reactivity, subassembly swap reactivity, foil activation measurement, integral reactivity coefficients, and analyses of sensitivity and uncertainty. About 30 international organizations from multiple member countries have participated in the CRP. Among the eight benchmark items, the results estimated by the participants for two items namely, reaction rate measurements from foil activations and integral reactivity coefficient, are compared and discussed in this paper.

Sixteen and ten international organizations participated in the reaction rate benchmark and evaluation of integral reactivity coefficients, respectively. The computation codes used include the deterministic codes of AZNHEX, DIF3D, ERANOS, JARFR, NAS, PARTISN, PARCS, SARAX, and stochastic codes of McCard, MCNP, MCS, MVP, OpenMC, RMC, and Serpent. Cross sections were generated from evaluated nuclear data libraries of ENDF/B (version VII.0, VII.1, and VIII.0), JEFF (version 3.1, 3.1.1, and 3.3), and JENDL (version 4.0).

For the reaction rate measurement by foil activations, a global agreement is observed in the fissile zone for the main axial and radial distributions. The convergence on the ^{197}Au at points far from the fissile core was difficult to be seen with both stochastic and deterministic codes. The thermal resonance needs accurate model for deterministic codes and good statistics for stochastic codes. Some improved results are seen in the refined phase (after disclosing of exact foil dimensions), indicating the positive effect of modelling accurately. Reaction rates on ^{235}U are in good agreement with the experiment throughout the profile, by most of the codes. Probable existence

of measurement (systematic) error is indicated in some cases where the codes agree with each other, but the measured value shows deviation, as could be seen in the results of Np^{237} and U^{238} reaction rates in radial position #8.

Stochastic and deterministic codes used in this study generally gave results in good agreement with the experiment, axially and radially. Attention is needed towards improved interpretation of experimental results and faithful reproduction of models in simulation for the following cases:

- reactions with low cross section (^{27}Al).
- reactions far from the fissile core, if the reaction rate is a threshold one (^{237}Np or ^{238}U).
- reactions with strong thermal resonance (^{197}Au).

For the integral reactivity coefficients, it is hard to assess the accuracy of the results because they were not measured in the CEFR start-up tests. Except for several outlier results, the predicted integral reactivity coefficients by participants are generally comparable regardless of deterministic and stochastic calculations. However, it was observed that the deterministic results have relatively larger standard deviations compared to the stochastic results. A wide diversity of deterministic methods (approximations of angular dependency, condensation of cross section, homogenization of geometry, etc.) could be the potential reason for larger standard deviations in the deterministic results.

ACKNOWLEDGEMENTS

Argonne National Laboratory's work was supported by the U.S. Department of Energy, Office of Nuclear Energy under contract DE-AC02-06CH11357. The data and information presented in this paper are part of an ongoing IAEA coordinated research project on "Neutronics Benchmark of CEFR Start-Up Tests – CRP-I31032."

REFERENCES

[1] HUO, X. (2019), "Technical Specifications for Neutronics Benchmark of CEFR Start-up Tests, Version 7.0," KY-IAEA-CEFRCRP-001, China Institute of Atomic Energy, December 2019.

[2] RIMPAULT, G., et al., "The ERANOS code and data system for reactor neutronic analyses", Proc. of PHYSOR 2002, Seoul, 2002, (2002).

[3] SANTAMARINA, A., et al., 2009. "The JEFF-3.1.1 nuclear data library". JEFF report, 22(10.2), 2.

[4] Paul K. Romano, Nicholas E. Horelik, Bryan R. Herman, Adam G. Nelson, Benoit Forget, and Kord Smith, "OpenMC: A State-of-the-Art Monte Carlo Code for Research and Development," *Ann. Nucl. Energy*, 82, 90–97 (2015).